Hurricane Model Experiments with a New Cumulus Parameterization Scheme

RICHARD A. ANTHES

Department of Meteorology, The Pennsylvania State University, University Park 16802

Manuscript received 22 July 1976, in revised form 19 November 1976)

ABSTRACT

A cumulus parameterization scheme that utilizes a one-dimensional cloud model is tested in a revised, axisymmetric hurricane model. The details of how the parameterization scheme may be incorporated into a larger scale model are presented. With a mean tropical sounding, the cumulus parameterization scheme yields a vertical distribution of heating that is appropriate for tropical cyclone development. The structure of the model hurricane and the properties of the convective clouds at various stages of the model storm development are described. The vertical distribution of the cloud-scale heating and the vertical eddy fluxes of heat, moisture and momentum are given as a function of radius from the storm center during the mature stage. The vertical fluxes of heat and moisture cool and dry the lower troposphere while they warm and moisten the upper troposphere. The vertical transport of radial momentum by the cumulus convection is relatively unimportant; however, the transport of tangential momentum is significant in reducing the vertical shear of the tangential wind.

1. Introduction

Three-dimensional hurricane models have produced realistic simulations of tropical cyclone development in recent years (Anthes *et al.*, 1971a; Anthes, 1972; Kurihara and Tuleya, 1974). The success of these idealized experiments and experimental forecasts by Miller *et al.* (1972) and Mathur (1974) have encouraged the development of an operational, primitive equation forecast model at the National Meteorological Center (Hovermale *et al.*, 1975). The above research and operational models have used simple cumulus parameterization schemes; Kurihara's model used a convective adjustment procedure while the others used some variation of Kuo's (1965, 1974) scheme. Although these schemes have proven adequate for representing the essential effects of cumulus convection on the hurricane's structure, they contribute little to the understanding of the interactions between the cumulus clouds and the larger scale circulations, as discussed by Anthes (1977), hereafter referred to as Paper I).

In Paper I we developed a cumulus parameterization scheme which utilized a one-dimensional cumulus cloud model. This model computes the cloud-scale heating distribution and the updraft thermodynamic properties that are necessary to determine the vertical eddy fluxes of heat and moisture in the larger scale model. This scheme provides a framework with which to study the response of individual clouds to the changing mesoscale thermal and moisture structures and the simultaneous influence of these convective elements on the evolution of the larger scale fields. Examples of the instantaneous effect of cumulus clouds on two different large-scale conditions were given. However, the proper testing of any parameterization scheme requires its use in a time-dependent, large-scale model where feedbacks between the convection and the environmental fields are permitted.

Two-dimensional (axisymmetric) hurricane models provide relatively inexpensive tools for testing numerical and physical schemes that do not depend on three dimensions (Anthes *et al.*, 1971b). In this paper, we test the cumulus parameterization scheme of Paper I in a revised axisymmetric hurricane model. A hurricane model provides a severe test of any cumulus parameterization scheme because unlike most other disturbances, hurricanes depend entirely upon latent heat release for their development and maintenance. Furthermore, as shown by Yamasaki (1968), Koss (1976) and others, the growth and structure of tropical cyclones is very sensitive to vertical variations in the latent heating distribution.

2. Description of the hurricane model

The axisymmetric hurricane model is a modified version of the two-dimensional model described by Anthes *et al.* (1971b). In addition to the revised cumulus parameterization scheme, the primary modifications, include a variable number of vertical layers, a modification of the vertical coordinate system to permit a nonzero upper pressure surface, and a modification of the finite-difference version of the hydrostatic equation.

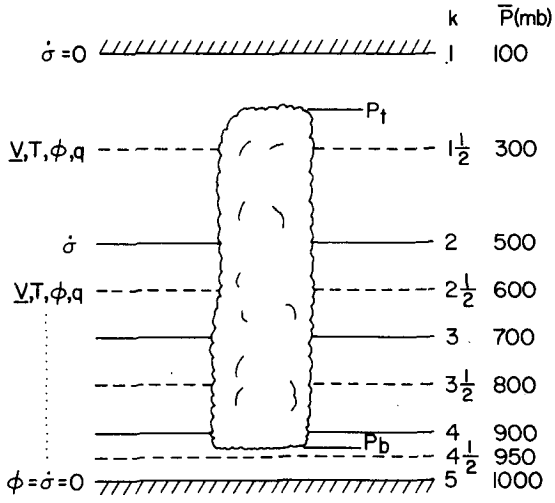

FIG. 1. Vertical structure of four-layer hurricane model.

a. The vertical structure of the model

The vertical coordinate σ is given by

$$\sigma=\frac{p-p_t}{p_s-p_t}, \tag{1}$$

where p is pressure, p_t the pressure at the top of the model and p_s the surface pressure. The vertical structure of the four-layer model used in this study is shown in Fig. 1. The choice of an upper pressure surface of 100 mb rather than zero as in the earlier model eliminates much of the ambiguity associated with representing the complex upper atmospheric structure including the tropopause by a single layer. In some preliminary experiments the model with $p_t=100$ mb produced a more realistic upper level storm structure than with $p_t=0$. This modification is particularly desirable when initializing models with real data.

The second modification involves the definition of geopotential ϕ and the calculation of ϕ from the hydrostatic equation for use in the computation of the horizontal pressure gradient force. Formerly (Anthes *et al.*, 1971b) ϕ was defined at the integer-k levels (Fig. 1). This scheme conserved total energy in the adiabatic, inviscid case but gave very large truncation errors near the top of the model when a small number of layers was used. A reduction of vertical truncation error and an improved storm structure were found when the geopotential was logarithmically integrated directly to the half-k levels.

b. The basic equations

The equations of motion in the σ-coordinate system under the assumption of axial symmetry may be written

$$\frac{\partial p^*u}{\partial t}=-\frac{1}{r}\frac{\partial rp^*u^2}{\partial r}+\frac{p^*v^2}{r}-p^*\frac{\partial \dot{\sigma}u}{\partial \sigma}+fvp^*-p^*\frac{\partial \phi}{\partial r}-\frac{RT}{[1+(p_t/p^*\sigma)]}\frac{\partial p^*}{\partial r}+F_H(u)+F_V(u), \tag{2}$$

$$\frac{\partial p^*v}{\partial t}=-\frac{1}{r}\frac{\partial rp^*uv}{\partial r}-\frac{p^*uv}{r}-p^*\frac{\partial \dot{\sigma}v}{\partial \sigma}-fup^*+F_H(v)+F_V(v), \tag{3}$$

where u and v are the velocity components in the radial (r) and tangential (λ) directions, respectively, $p^*=(p_s-p_t)$, T is temperature and f is the Coriolis parameter (here equal to 5×10^{-5} s^{-1}).

The terms F_H (u,v) and F_V (u,v) in (2) and (3) represent the horizontal and vertical redistribution of momentum by small-scale turbulent eddies and cumulus convection, and are discussed later.

The continuity and thermodynamic equations are

$$\frac{\partial p^*}{\partial t}=-\frac{1}{r}\frac{\partial}{\partial r}(rp^*u)-\frac{\partial p^*\dot{\sigma}}{\partial \sigma}, \tag{4}$$

$$\frac{\partial p^*T}{\partial t}=-\frac{1}{r}\frac{\partial rp^*uT}{\partial r}-p^*\frac{\partial \dot{\sigma}T}{\partial \sigma}+\frac{RT\omega}{c_p(\sigma+p_t/p^*)}+p^*\frac{\partial T}{\partial t_c}+p^*F_H(T)+\frac{p^*}{c_p}\dot{Q}_{\text{sea}}\ \text{(lowest layer only)}, \tag{5}$$

where $\partial T/\partial t_c$ represents the change of temperature due to cumulus convection and $\omega\equiv dp/dt$ is

$$\omega=p^*\dot{\sigma}+\sigma\frac{dp^*}{dt}. \tag{6}$$

The term $\dot{Q}_{\text{sea}}$ is the diabatic heating rate per unit mass associated with sensible heat flux at the sea surface and is calculated according to standard exchange coefficient theory (Anthes *et al.*, 1971a).

The hydrostatic equation is

$$\frac{\partial \phi}{\partial \ln(\sigma+p_t/p^*)}=-RT, \tag{7}$$

where R is the gas constant for dry air.

The continuity equation for water vapor is given by

$$\frac{\partial p^*q}{\partial t}=-\frac{1}{r}\frac{\partial rp^*uq}{\partial r}-p^*\frac{\partial \dot{\sigma}q}{\partial \sigma}+p^*F_H(q)-p^*\bar{C}^*+E_{\text{sea}}\ \text{(lowest layer only)}, \tag{8}$$

where $\bar{C}^*$ represents the sink of moisture associated with the area average of the cloud-scale condensation

rate [see (23) of Paper I] and E_{sea}, defined by (35), represents evaporation from the sea. The water vapor cycle is described in Section 3c.

c. The finite-difference equations

The finite-difference equations for (2)–(6) are identical to those presented by Anthes *et al.* (1971b) and are not given here. However, as discussed earlier, the finite difference for the hydrostatic equation (7) was modified to give a more accurate integration of ϕ. At the lowest velocity level ϕ is given by

$$\phi_{4\frac{1}{2}}=R\bar{T}\ln\frac{\sigma_5+c_1}{\sigma_{4\frac{1}{2}}+c_1}, \tag{9}$$

where $c_1=p_t/p^*$ and the mean temperature represents the average in the layer from $\sigma_{4\frac{1}{2}}$ to σ_5. Because temperature is not predicted at the σ_5 level, it is obtained by a downward extrapolation from the $\sigma_{4\frac{1}{2}}$ level according to

$$T_5=T_{4\frac{1}{2}}+3.6°\text{C}. \tag{10}$$

For the rest of the levels, the geopotential is computed from

$$\phi_{k-\frac{1}{2}}=\phi_{k+\frac{1}{2}}+R\bar{T}_k\ln\frac{\sigma_{k+\frac{1}{2}}+c_1}{\sigma_{k-\frac{1}{2}}+c_1}, \quad k=4, 3, 2, \tag{11}$$

where $\bar{T}_k$ is the arithmetic average of the temperatures at levels $(k-\frac{1}{2})$ and $(k+\frac{1}{2})$.

d. Horizontal diffusion of momentum

The horizontal diffusion of momentum in (2) and (3) is given by

$$F_H(u)=\frac{\partial K_H\dfrac{\partial u}{\partial r}}{\partial r}+\frac{K_H}{r}\frac{\partial u}{\partial r}-\frac{K_H u}{r^2} \tag{12}$$

with a similar expression for v. The horizontal diffusion terms for temperature and water vapor are

$$F_H(T)=\frac{\partial rK_H\dfrac{\partial T}{\partial r}}{r\partial r} \tag{13}$$

with a similar expression for q.

In (12) and (13), K_H is the variable horizontal eddy diffusivity for momentum, i.e.,

$$K_H=K_{H_0}+\tfrac{1}{2}k_0^2(\Delta r)^2|D|, \tag{14}$$

where K_{H_0} is 2.5×10^4 m^2 s^{-1}, Δr is the horizontal grid spacing, $k_0=0.4$, and the deformation D in an axisymmetric system is

$$D=r\left[\left(\frac{\partial u/r}{\partial r}\right)^2+\left(\frac{\partial v/r}{\partial r}\right)^2\right]^{\frac{1}{2}}. \tag{15}$$

Except for the constant term K_{H_0} in (14) the horizontal diffusion is equal to that given by Smagorinsky *et al.* (1965). It is noteworthy that the form of the horizontal diffusion term for momentum given by Anthes *et al.* (1971b) is only an approximation to the exact form (12) if K_H varies, i.e.,

$$\frac{1}{r^2}\frac{\partial}{\partial r}\left(K_H r^3\frac{\partial \mathrm{V}/r}{\partial r}\right)=\frac{\partial}{\partial r}\left(K_H\frac{\partial \mathrm{V}}{\partial r}\right)+\frac{K_H}{r}\frac{\partial \mathrm{V}}{\partial r}-\frac{K_H\mathrm{V}}{r^2}-\frac{\mathrm{V}}{r}\frac{\partial K_H}{\partial r}. \tag{16}$$

The approximate form, given by the left side of (16), is equal to the exact form, given by the first three terms on the right of (16), plus the additional term involving the radial variation of K_H. In a comparison experiment with the old cumulus parameterization scheme using the exact and approximate forms, a significant difference in the radial profile of the wind was noted near the radius of maximum wind (Fig. 2).

e. Vertical diffusion of momentum

The vertical redistribution of momentum by scales smaller than those resolvable by the model falls into two categories, the vertical transport associated with deep cumulus clouds and the vertical diffusion associated with subcumulus-scale eddies. These processes may be written schematically as

$$\mathbf{F}_V=-g\frac{\partial \boldsymbol{\tau}_s}{\partial\sigma}-g\frac{\partial \boldsymbol{\tau}_c}{\partial\sigma}, \tag{17}$$

where $\boldsymbol{\tau}_s$ represents the vector stress associated with the small-scale turbulent eddies and $\boldsymbol{\tau}_c$ refers to the stresses associated with the momentum transport in the cumulus clouds.

The turbulent fluxes of momentum by the small-scale eddies, represented by $\boldsymbol{\tau}_s$ in (17), are very similar to those in Anthes *et al.* (1971). At the lowest level of the model $\boldsymbol{\tau}_s$ is

$$\boldsymbol{\tau}_s=\rho^*C_D|\mathbf{V}_4|\mathbf{V}_4, \quad k=5, \tag{18}$$

where the drag coefficient C_D is 3.0×10^{-3} and the surface density ρ^* is 1.1 kg m^{-3}. For levels 2–4, $\boldsymbol{\tau}_s$ is

$$\boldsymbol{\tau}_s=\rho K\frac{\partial \mathbf{V}}{\partial z}, \quad k=2\text{–}4, \tag{19}$$

where ρ is density, z is height, and K is the kinematic coefficient of eddy viscosity here equal to

$$K=25.0+2\times10^4\left|\frac{\partial \mathbf{V}}{\partial z}\right|, \tag{20}$$

where the wind shear is expressed in s^{-1} and K is in m^2

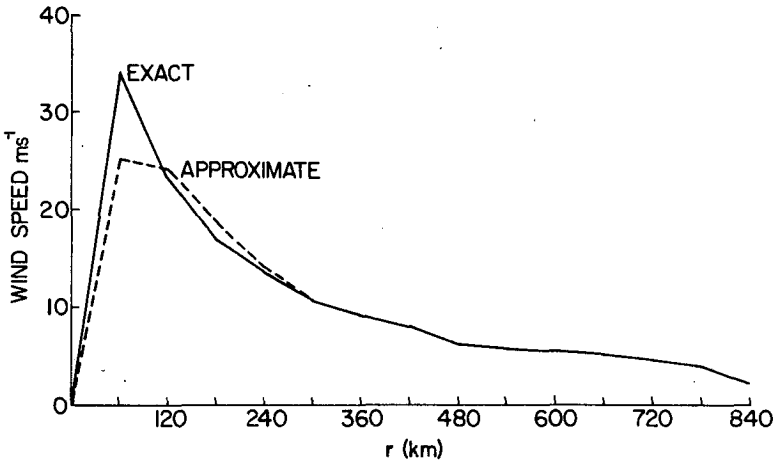

FIG. 2. Radial profiles of wind speed at lowest level (~950 mb) at 48 h from experiments using exact form of horizontal diffusion (solid line) and approximate form (dashed line).

s^{-1}. This formulation for vertical mixing was established by trial and error. The maximum values of K during the most intense phase of the storm reach about 150 $m^2 s^{-1}$.

The effect of the vertical flux of momentum by the cumulus clouds on the resolvable scale, derived by the methods in Paper I, is

$$\tau_c=\frac{1}{g}\overline{-\omega'\mathbf{V}'}=\frac{a(\omega_c-\omega)(\mathbf{V}_c-\mathbf{V})}{g(1-a)}, \tag{21}$$

where the c subscript refers to the cumulus cloud, the variables without subscripts represent horizontal averages over a grid area, and a is the fraction of the grid area covered by cumulus clouds. The cumulus vertical velocity ω_c is obtained from a one-dimensional cumulus cloud model (see Paper I). The horizontal velocity in the cumulus cloud is obtained by consideration of the entrainment of mean horizontal momentum into the cloud. In this simplified approach, which neglects horizontal accelerations produced by perturbations in the horizontal pressure gradient force, the cloud is assumed to conserve the horizontal momentum at cloud base except for the entrainment of momentum from different layers of the model as the cloud passes through these layers. The vertical rate of change of any updraft property α_c due to entrainment is

$$\frac{d\alpha_c}{dz}=\frac{1}{M}\frac{dM}{dz}(\alpha_c-\alpha_e), \tag{22}$$

where M is the mass flux of the updraft, α_e the value of α in the environment and $(1/M)(dM/dz)$ the entrainment rate. Given α_c at some level k in the model, the value of α_c at the next higher level $(k-1)$ is given by a finite-difference approximation to (22), i.e.,

$$\alpha_c(k-1)=\frac{M_k\alpha_c(k)+\Delta M\bar{\alpha}_e}{M_k+\Delta M}, \tag{23}$$

where M_k is the mass flux at level k, ΔM the increase in mass flux in the layer between levels k and $k-1$ and $\bar{\alpha}_e$ the mean value of α_e in that layer. The mass entrained is obtained from the one-dimensional cloud model (see Paper I). The horizontal momentum $\mathbf{V}_c$ in the cloud is obtained from (23) with the assumption that the momentum at cloud base equals the mean horizontal momentum at that level. Because the percent area covered by convection is assumed small, the environmental values of momentum are approximated by the area-averaged values.

f. Time integration, lateral boundary and initial conditions, and horizontal resolution

The time integration scheme is the Matsuno (1966) simulated backward scheme, which damps high temporal frequencies. The boundary conditions at the edge of the 960 km radial domain consist of steady-state pressure, temperature and specific humidity. Under inflow conditions, the horizontal velocity components are specified to be zero; under outflow conditions they are extrapolated outward with the assumptions of zero divergence and relative vorticity. The initial conditions consist of a barotropic vortex in gradient balance with a maximum wind of 18 m s^{-1} at a radius of 240 km. The horizontal grid size Δr is arbitrary; here it is 30 km for $r \leqslant 300$ km and 60 km beyond this radius. The time step for this resolution is 37.5 s.

3. Implementation of the cumulus parameterization scheme

Because the cumulus parameterization scheme tested in this paper is fully described in Paper I, only the details of its implementation in the hurricane model are presented here.

a. Meshing of cloud and hurricane model structures

A schematic diagram of the cloud model and its interaction with the hurricane model is shown in Fig. 3. In the hurricane model, the contribution to the thermodynamic equation (5) by the cumulus convection is

$$\frac{\partial T}{\partial t_c}=\frac{L}{c_p}\bar{C}^*_{k+\frac{1}{2}}-\frac{\partial\overline{\omega'T'}}{\partial p}. \tag{24}$$

The heating function $\partial T/\partial t_c$ is required at the half-k levels, while the eddy fluxes of heat, moisture and momentum are defined at the whole-k levels. In the discrete model $\bar{C}^*_{k+\frac{1}{2}}$ is the vertical average of $\bar{C}^*$ in the layer bounded by σ_k and σ_{k+1}. This cloud-scale condensation rate is obtained from the cloud model, with $\bar{C}^*=0$ below the cloud base or above the cloud top.

The cumulus-scale condensation rate in the discrete hurricane model, in finite-difference form analogous to (27) in Paper I, is

$$\bar{C}^*_{k+}=\frac{(1-b)gM_tN_{k+\frac{1}{2}}}{(P_b-P_u)}, \tag{25}$$

where P_b and P_u are the pressure levels at cloud base and top, respectively, and M_t is the total water vapor convergence in a column [see (29)]. The fraction b of water vapor convergence that is not precipitated out is given by (58) in Paper I with $n=1$ and $\mathrm{RH}_c=0.50$. The vertical distribution function is

$$N_{k+\frac{1}{2}}=\langle\bar{C}^*\rangle^{-1}\left[(p_{k+1}-p_k)^{-1}\int_{p_k}^{p_{k+1}}\bar{C}^*(p)dp\right], \tag{26}$$

where the vertical-averaging operator $\langle\ \rangle$ of any quantity χ is defined by

$$\langle\chi\rangle=(P_b-P_u)^{-1}\int_{p_t}^{p_s}\chi dp. \tag{27}$$

The integrals in (26) and (27) are evaluated from the cloud model by numerical quadrature. The conservation of latent energy in this step is demonstrated by summing (24) over all layers of the model after multiplying by the mass in each layer, i.e.,

$$g^{-1}\int_{p_t}^{p_s}c_p\frac{\partial T}{\partial t_c}dp\approx c_pg^{-1}\sum_{k=1}^{4}\frac{\partial T}{\partial t_c}(p_{k+1}-p_k)=(1-b)LM_t. \tag{28}$$

b. Calculation of clouds from time-averaged model properties

The heating rates and cloud variables ω_c, T_c and q_c obtained from the cloud model represent average properties of a representative cumulus cloud over each grid area. To help ensure that a representative cloud is produced, the temperatures and specific humidities predicted by the hurricane model at each level are averaged over a time interval τ_c, where τ_c is on the order of the characteristic lifetime of the cumulus cloud. This time-averaged, large-scale sounding is used as input in the cloud model. The cloud properties thus obtained are then utilized in the hurricane model for the next τ_c seconds at which time a new cloud is generated. In this experiment τ_c is 1 h, so that with a time step of 37.5 s, a cumulus cloud is computed every 96 time steps. This procedure makes the cumulus parameterization scheme quite economical, adding only about 10% to the entire computation time.

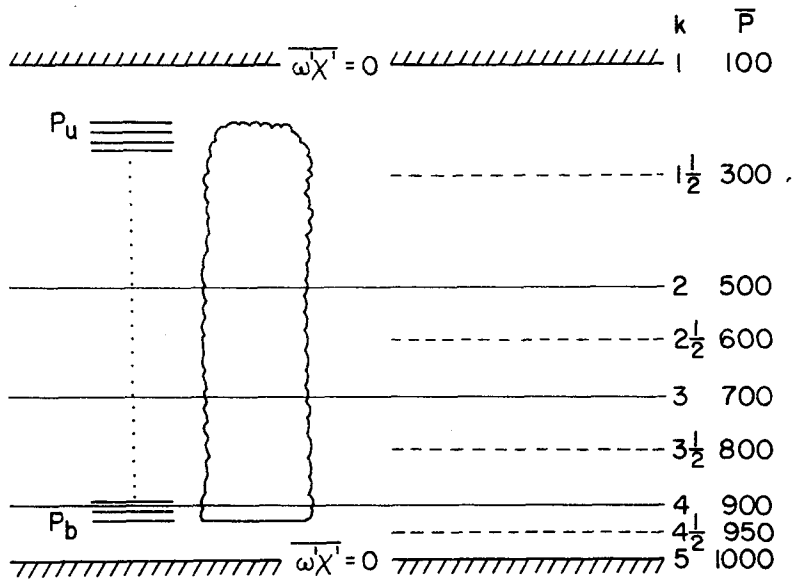

FIG. 3. Schematic diagram showing relationship between cloud model structure and hurricane model structure.

In order to generate a high-resolution sounding for the cloud model, departures of temperature and relative humidity from a reference sounding [here the Gulf of Mexico mean hurricane season sounding (Hebert and Jordan, 1959)] are computed at each level in the hurricane model and linearly interpolated to the necessary levels in the cloud model (Fig. 3). The departures from the reference sounding are assumed to vanish at the upper pressure surface in the hurricane model.

c. Water vapor equation

Cumulus convection is assumed to occur in any column in which the vertically integrated moisture convergence M_t exceeds a critical value (here taken to be 10^{-2} gm m^{-2} s^{-1})[1] and the cloud model predicts a cloud top of at least 700 mb.[1] Here M_t is defined by

$$M_t=-\frac{1}{g}\int_0^1 \nabla\cdot p^*\mathbf{V}q d\sigma. \tag{29}$$

Under these conditions, the moisture equation is

$$\frac{\partial p^*q}{\partial t}=p^*\frac{\partial q^+}{\partial t}-p^*\frac{\partial\overline{\omega' q'}}{\partial p}\equiv p^*\frac{\partial q}{\partial t_c}, \tag{30}$$

where $\partial q^+/\partial t$ is the moistening effect of the convection. Note that E_{sea} is added to (30) at level $k=4\frac{1}{2}$. The expression for $\partial q^+/\partial t$ in the discrete model is

$$\left(\frac{\partial q^+}{\partial t}\right)_{k+\frac{1}{2}}=\frac{bgM_tN'_{k+\frac{1}{2}}}{(P_b-P_u)}, \tag{31}$$

where the vertical distribution function N' for the moistening is (Paper I)

$$N'_{k+\frac{1}{2}}=\langle(100\%-\text{RH})q_s\rangle^{-1}\left[(p_{k+1}-p_k)^{-1}\times\int_{p_k}^{p_{k+1}}(100\%-\text{RH})q_s dp\right]. \tag{32}$$

Here RH is the relative humidity and q_c the saturation specific humidity at the temperature of level $k+\frac{1}{2}$.

The conservation of latent energy from the moistening term may be demonstrated by summing over all layers

$$g^{-1}\int_{p_t}^{p_s}L\frac{\partial q^+}{\partial t}dp\approx Lg^{-1}\sum_{k=1}^{4}\frac{\partial q^+}{\partial t}(p_{k+1}-p_k)=bLM_t. \tag{33}$$

Eqs. (33) and (28) show that in columns with convection

$$\sum_{k=1}^{4}\left(c_p\frac{\partial T}{\partial t_c}+L\frac{\partial q}{\partial t}\right)(p_{k+1}-p_k)=gLM_t, \tag{34}$$

which demonstrates the conservation of latent energy in the cumulus parameterization scheme.

In columns which do not support cumulus convection, the full continuity equation for water vapor (8) is used with $\bar{C}^*$ equal to zero. The flux convergence of water vapor in the lowest layer associated with evaporation from the sea surface is

$$E_{\text{sea}}=\begin{cases}gC_E|\mathbf{V}_{4\frac{1}{2}}|\rho^*(q_{\text{sea}}-q^*)/(\sigma_5-\sigma_4), & q_{\text{sea}}>q^*\\ 0, & q_{\text{sea}}\leqslant q^*\end{cases} \tag{35}$$

where q_{sea} is the saturation specific humidity at the sea temperature and the exchange coefficient C_E is equal to the drag coefficient C_D. The specific humidity q^* at "anemometer level" is obtained by a downward extrapolation of the relative humidity and temperature from level $4\frac{1}{2}$ subject to the constraint that the surface relative humidity not exceed 95%.

d. Summary of water vapor and convective parameterization cycle

The water vapor cycle, which includes the cumulus parameterization scheme, is outlined in Fig. 4. New cloud properties are computed every τ_c seconds. During the remaining time steps, the cloud properties computed from the previous cloud calculation are utilized while the instantaneous temperatures and specific humidities from the hurricane model are accumulated for use in the next cloud calculation. If the cloud top is above 700 mb and the vertically integrated moisture convergence exceeds the critical value, the convective contributions to the thermodynamic and moisture equations are computed and (30) is used to compute the moisture tendency. Otherwise the convective tendencies are set to zero and (8) is used for the moisture prediction equation. Finally, the tentative forecasts for T and q at the next time step are made. If any supersaturated layers exist at this point, T and q are simultaneously adjusted to produce a relative humidity of 100%. The moisture condensed in this step is referred to as large-scale or nonconvective heating.

4. Numerical results

An experiment with 60 km horizontal resolution everywhere and another with 30 km resolution inside the 300 km radius were run for 96 h with the new cumulus parameterization scheme. The time variation of the maximum wind speed is shown in Fig. 5. After the first 12 h, the experiment with the higher horizontal resolution in the interior shows faster wind speeds. The structure of the two experiments are quite similar, however, so that only the high-resolution results are discussed here.

a. Structure of the mature model storm

After a brief weakening period when the sudden introduction of surface friction destroys the initial

[1] This value is equivalent to a rainfall rate of about 0.09 cm day^{-1}.

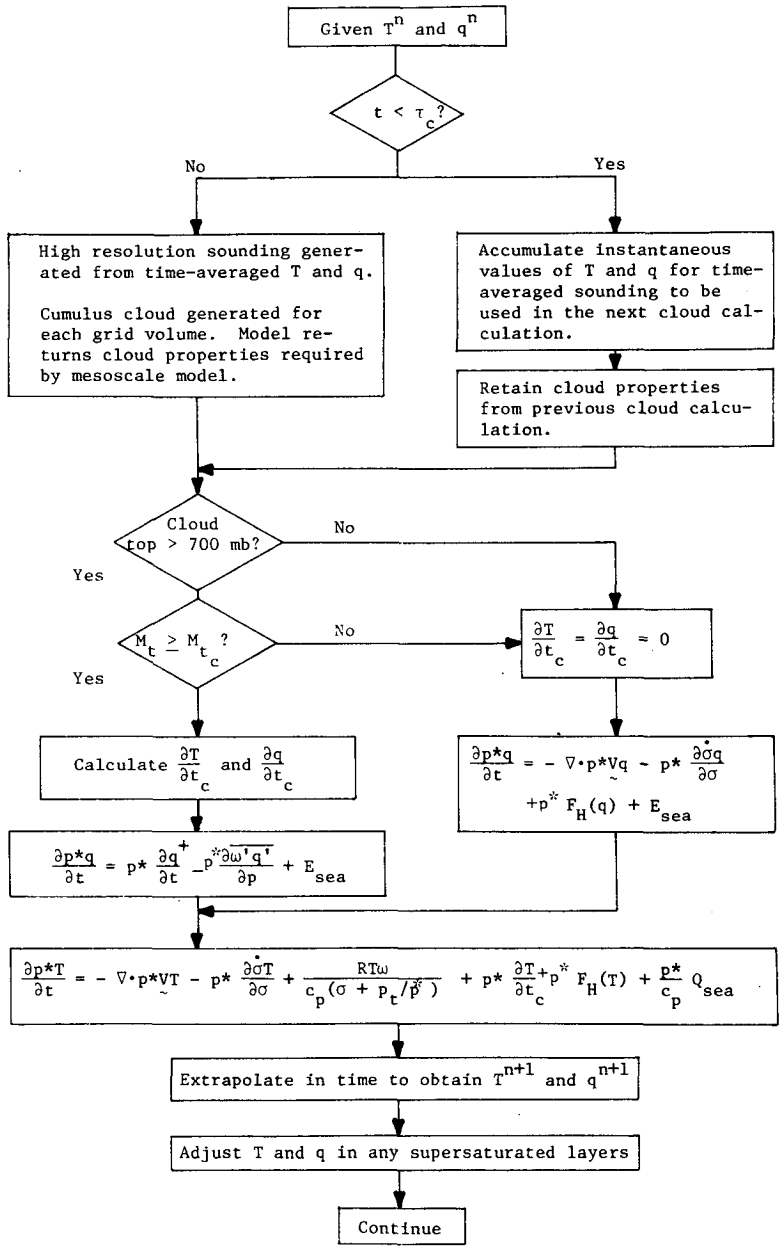

FIG. 4. Outline of water vapor cycle and cumulus parameterization scheme.

gradient balance, the model storm intensifies rapidly to reach a maximum wind of 30 m s^{-1} at 24 h. A second period of slow intensification begins around 36 h and continues until about 84 h, when a quasi-steady state is attained. The maximum winds are about 45 m s^{-1} at this time.

The vertical cross sections of wind speed, temperature anomaly (departure of temperature from initial conditions) and relative humidity at 72 h are shown in Fig. 6. The structure of the storm at this time is typical of the model storm during the last 48 h of the forecast. The wind speed cross section shows a maximum of 43 m s^{-1} at about 130 km. A warm temperature anomaly dominates the inner region with a temperature excess of nearly 10°C. Slight cooling is observed in the lower troposphere inside the 120 km radius.

The relative humidity cross section shows a large moist region in the middle and upper troposphere in the vicinity of the maximum winds and a thin moist boundary layer. The high relative humidities in the boundary layer indicate that evaporation is overestimated, probably because of the use of a constant exchange coefficient. The dry layer in the middle troposphere beyond the radius of maximum wind is a result of subsidence.

Compared to previous axisymmetric model results (Anthes *et al.*, 1971b) the model storm in this experi-

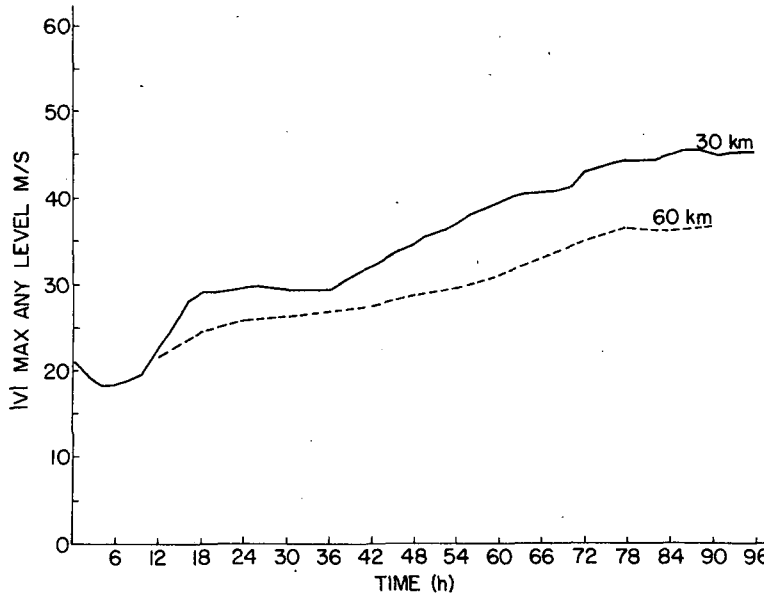

FIG. 5. Maximum wind speed as a function of time in hurricane experiments using new cumulus parameterization scheme. The experiments are identical except for the horizontal resolution, which is either 30 or 60 km inside the 300 km radius.

ment is considerably larger, with the maximum wind (estimated by interpolation) at a radius of about 130 km at 72 h. The storm expands after 30 h, with the radius of gale force (22 m s^{-1}) and hurricane force (33 m s^{-1}) winds steadily increasing during this period (Fig. 7). The storm structure at 72 h is bigger than most real storms, although some of the larger storms approach this size. For example, Hurricane Ginger (1971) had a radius of maximum wind between 74 and 93 km on 26 September 1971 (Bergman and Carlson, 1975). Although real hurricanes vary tremendously in size, very little is known about the physical causes for the variation. However, factors that are important in determining the size of model storms, in addition to the cumulus parameterization scheme, include the formulation of the drag coefficient, the air-sea exchange

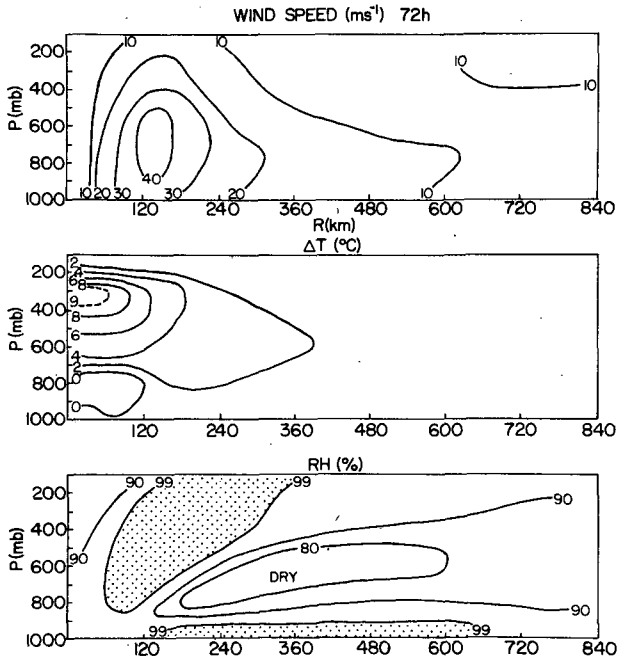

FIG. 6. Vertical cross sections of wind speed, temperature anomaly and relative humidity at 72 h.

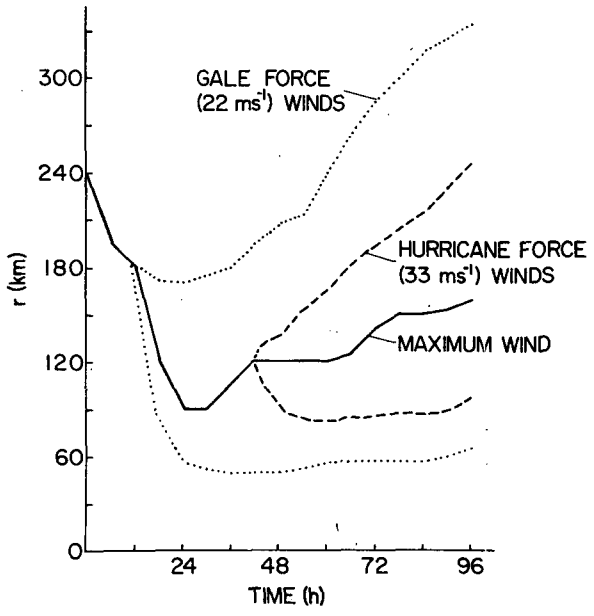

FIG. 7. Time variation of radii of maximum wind, gale force winds (22 m s^{-1}) and hurricane force winds (33 m s^{-1}).

coefficient, the Coriolis parameter and the horizontal diffusivity of momentum (Rosenthal, 1970, 1971).

b. Interaction of cumulus convection and the mesoscale hurricane circulation

A major purpose of this paper is to study the interactions between the cumulus clouds and the hurricane circulation as represented by the new cumulus parameterization scheme. The time-dependent behavior of some of the important parameters in the scheme is shown in Fig. 8. These parameters all pertain to the column of maximum convective heating.

The curves labeled ⟨RH⟩ and b denote the vertically averaged relative humidity and the percent of total moisture convergence that is not precipitated out. This portion moistens the lower portion of the column against the drying effects of the vertical eddy flux of moisture by convection. The average relative humidity varies between 90 and 98% with b ranging from 8 to 15%. Thus, in the region of intense moisture convergence, most of the convergence is precipitated out immediately.

As discussed in Paper I, the growth and structure of model hurricanes depend critically on the vertical partitioning of the latent heating, which is summarized by two parameters l (Yamasaki, 1968) and W (Koss, 1976):

$$l=\int_{600}^{p_s} Q\,dp \Big/ \int_{0}^{p_s} Q\,dp, \tag{36}$$

$$W=\int_{0}^{450} Q\,dp \Big/ \int_{0}^{p_s} Q\,dp, \tag{37}$$

where Q is the total diabatic heating rate per unit mass.

According to linear analyses by Yamasaki (1968) and Koss (1976), model storms that have structures like tropical cyclones develop for values of l from 0.3 to 0.45 and W from 0.47 to 0.53. These parameters are shown as a function of time in Fig. 8. The greatest contribution to these parameters is the cloud-scale heating rate. The vertical eddy flux of heat and the nonconvective heating shift the total heating maximum upward, thereby reducing l and increasing W. The values of l and W in the hurricane model are close to the values found by Yamasaki and Koss to give realistic tropical cyclones, and indicate that the cumulus parameterization scheme is capable of producing realistic convective heating rates. Values of l and W at the radius of maximum convection are remarkably constant during the integration in spite of the changing thermal structure of the storm.

Finally, the percent a of area covered by cumulus updrafts is computed according to three different methods. These estimates are graphed as a function of time in Fig. 8. The graph titled "cloud a" depicts a computed from the new parameterization scheme according to (44) in Paper I. This value was used in computing the eddy flux terms such as (21). For comparison, two other methods of estimating a were computed. In the method proposed by Kuo (1965, 1974), a is computed from

$$a=\frac{TM_t}{M_c}, \tag{38}$$

where T is the half-life of a cloud (~1 h) and M_c the total energy (internal and latent) needed to convert an entire column at initial temperature T and specific humidity q to a "cloud" temperature T_c and specific

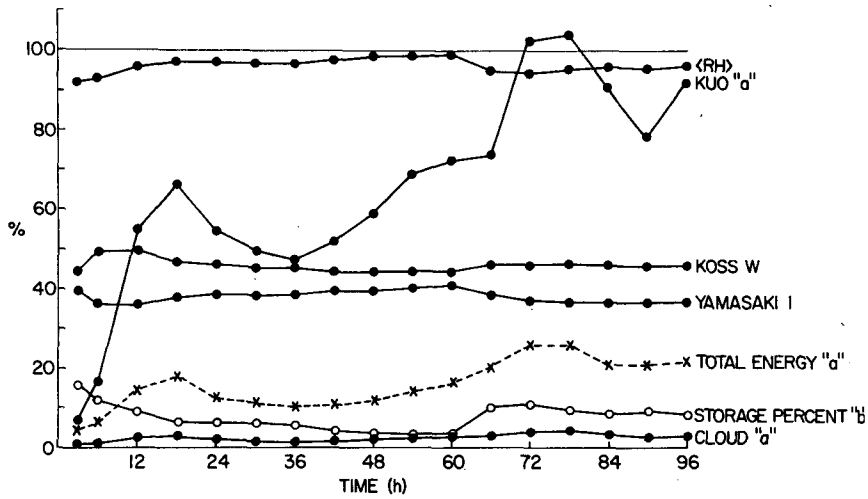

FIG. 8. Time variation of various parameters at the radius of maximum convective heating. Included are the mean relative humidity in the column (⟨RH⟩), the percent a of area covered by cumulus convection computed by three methods (see text), the parameters W and l (again see text), and the percent of the total moisture convergence that is utilized in moistening rather than heating the column.

humidity q_c, i.e.,

$$M_c \equiv g^{-1}\int_{p_t}^{p_s}\left[\frac{c_p}{L}(T_c-T)+(q_c-q)\right]dp. \quad (39)$$

The essential assumption in deriving Kuo's expression is that all of the water vapor convergence in the time period T is utilized in the production of air with the new properties T_c and q_c. However, in an open system, much of the water vapor convergence may be converted to internal and potential energy and exported out of the column rather than used to convert the column to the new temperature and humidity.

A modification to Kuo's method of estimating a, here called the total energy method, replaces the total moisture convergence M_t in (38) with L^{-1} times the total energy convergence E_T defined by

$$E_T = g^{-1}\int_0^{p_s}\nabla\cdot[\mathbf{V}(C_pT+gz+Lq)]dp + L\rho^* C_E|\mathbf{V}_{4\frac{1}{2}}|(q_{\text{sea}}-q^*)+C_p\rho^* C_E|\mathbf{V}_{4\frac{1}{2}}| \times(T_{\text{sea}}-T^*). \quad (40)$$

In an open system with low-level convergence and upper level divergence, E_T will be considerably less than M_t because internal and potential energy will be exported from the column in the upper troposphere, offsetting to some extent the low-level moisture convergence. The modified scheme, however, suffers from the same drawbacks as Kuo's scheme, namely that the T parameter is arbitrary and that the utilization of the total energy convergence may take other forms than the hypothesized conversion of the column to the specified temperature and mixing ratio.

The values of a computed by Kuo's water vapor convergence method and the total energy convergence method are presented in Fig. 8. Kuo's method greatly overestimates a; in fact a exceeds 100% between 72 and 78 h. The value of a computed according to the total energy convergence method is considerably smaller, showing a maximum value of only 26%. However, the values are still much greater than those computed from the revised cumulus parameterization scheme. These latter values are considered most realistic, since the estimates of the percent area covered by active updrafts, even near the center of hurricanes, are typically a few percent (Malkus *et al.*, 1961).

1) The structure of cumulus clouds near the hurricane center

The vertical profiles of cloud temperature excess (T_c-T) and vertical motion W computed from the cloud model at 3, 36 and 72 h at a radius of 15 km are shown in Fig. 9. At 3 h the conditional instability is large and the updraft reaches a maximum vertical velocity of 21 m s^{-1}. The maximum updraft occurs at 450 mb while the level of maximum temperature excess is about 600 mb.

As the storm intensifies and the upper level warm core develops, the conditional instability is reduced. By 36 h the cloud temperature excess at the 600 mb level is reduced to less than 1°C and the vertical velocity profile shows a considerable reduction in the layer from 650 to 250 mb. By 72 h the temperature excess at 300 mb is reduced to nearly zero and only the cloud's inertia carries it through this stable layer. At 84 h (not shown), the upper troposphere has warmed so much that convection is able to reach only the 400 mb level.

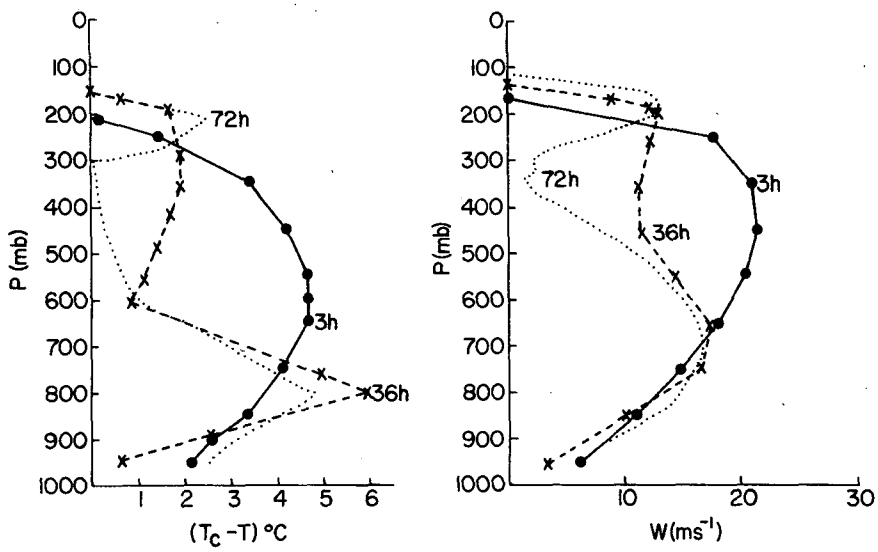

FIG. 9. Cloud temperature excess (T_c-T) and vertical velocity W from cumulus model at a radius of 15 km in hurricane model at 3, 36 and 72 h.

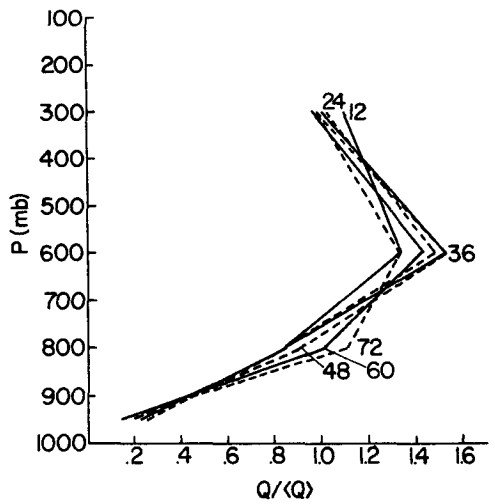

FIG. 10. Vertical distribution of normalized total latent heating function at radius of maximum heating for various times.

2) THE TIME VARIATION OF THE VERTICAL HEATING DISTRIBUTION

In spite of the large changes in temperature and moisture structure of the model hurricane, the variation with time of the vertical heating function is fairly small, as already indicated by the relatively constant l and W parameters (Fig. 8). The normalized vertical distribution of the total latent heating function Q at the radius of maximum heating is

$$Q'=Q/\langle Q\rangle \tag{41}$$

and is shown in Fig. 10 at 12, 24, 36, 48, 60 and 72 h. There is a slight tendency for the total heating maximum to shift to lower levels as the upper layers become warmer and the upper portion of the clouds become weaker. However, the variation is much less than would be expected from the time variations of (T_c-T) at the radius of maximum convection, as shown in Fig. 11. Here the maximum in the normalized (T_c-T) profile shifts from 600 mb at 12 h to 800 mb at 36 h. Thus, while the normalized (T_c-T) profile is very similar to the actual heating distribution early in the model storm's life, it is very much different from the actual distribution in the mature stage of the storm.

3) CONVECTIVE HEATING AND VERTICAL EDDY TRANSPORTS DURING THE MATURE STAGE

The effect of cumulus convection on the hurricane's thermodynamic and moisture fields is shown in Fig. 12. These cross sections are representative of the last 48 h of the integration.

Fig. 12a shows the vertical and horizontal distribution of the area-averaged convective heating, which is the largest diabatic heating term. Individual temperature-change rates of over 300°C day^{-1} occur in the mid-troposphere at a radius of 120 km.

The magnitude of the divergence of the vertical eddy heat flux, shown in Fig. 12b, is about an order-of-magnitude smaller than the convective heating term. The vertical eddies cool a thin layer near cloud base at a rate of 40°C day^{-1} and warm a thicker upper tropospheric layer at a rate of 20°C day^{-1}.

The nonconvective heating, shown in Fig. 12c, results mainly from the upward flux of water vapor by the cumulus eddy flux term, which is shown in Fig. 12d. Nonconvective heating is defined as the condensation heating associated with large-scale motions rather than cumulus-scale motions. The nonconvective rates exceed 60°C day^{-1} in the middle troposphere. Although the heating by the vertical eddy fluxes and the nonconvective heating are considerably smaller than the convective heating, they both act to shift the maximum in the total heating upward. Thus the realistic vertical partitioning of the total heating distribution, as measured by the parameters l and W, is a result of all three terms. Without the correction associated with the eddy fluxes and nonconvective heating, l would be too large and W too small for realistic tropical cyclone development.

The divergence of the vertical eddy moisture flux, shown in Fig. 12d, is a very important term in the moisture equation and, as discussed above, provides a source of water vapor for the nonconvective heating in the middle and upper troposphere. This process also has an important drying effect in the lower troposphere; it removes water vapor from the boundary layer at a rate of over 60×10^{-3} day^{-1}. By drying the boundary layer and making evaporation from the sea more vigorous, this term indirectly increases the intensity of the storm.

The last convective term shown in Fig. 12 is the moistening term associated with cumulus convection, $\partial q^+/\partial t$. This term represents both evaporation effects around and under cumulus clouds and the portion of the

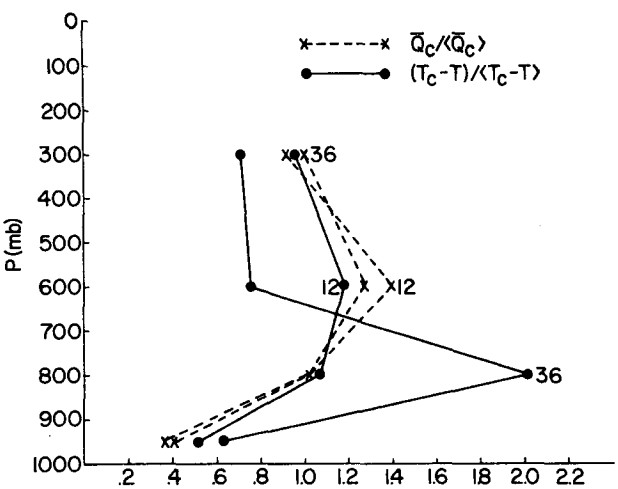

FIG. 11. Vertical distribution of normalized cloud-scale condensation heating and nomalized distribution of (T_c-T) at a radius of 15 km at 12 and 36 h.

total water vapor convergence that is never condensed in the column. It is essentially proportional to the departure of the specific humidity in a layer from the saturation value. As shown in Fig. 12e, the greatest effect is in the lower troposphere where the specific humidity deficit is greatest. This term counteracts the drying effect of the vertical eddy flux of water vapor in this layer.

4) VERTICAL FLUX OF MOMENTUM BY CUMULUS CONVECTION

The contributions to the equation of motion by the vertical eddy fluxes of momentum at 72 h are shown in Figs. 13a and 13b and the radial and tangential velocity cross sections at the same time are shown in Figs. 13c and 13d. The effect on the radial momentum is relatively straightforward to interpret. The upward transport of negative radial wind component (inflow) acts to reduce the circulation in the r-z plane by opposing the low-level inflow and the upper-level outflow. However, this term is less than 10% of the centripetal acceleration v^2/r in this region.

The effect of the cumulus eddy transports on the tangential equation of motion (3) is more significant, because it is comparable in magnitude to the other terms. The cumulus clouds transport cyclonic momentum away from the maximum which occurs around 700 mb, thereby increasing v above and below this level. Thus cumulus convection tends to redistribute tangential momentum in the vertical as suggested by Gray (1967).

5. Summary

A new cumulus parameterization scheme that utilizes a one-dimensional cloud model has been tested in a two-dimensional hurricane model. Although the model hurricane was somewhat larger than real storms, its structure was typical of real storms in many respects and demonstrated that the cumulus parameterization scheme provides realistic results in a hurricane model. The vertical distribution of heating produced by the cumulus parameterization scheme was typical of that which is necessary for tropical cyclone development.

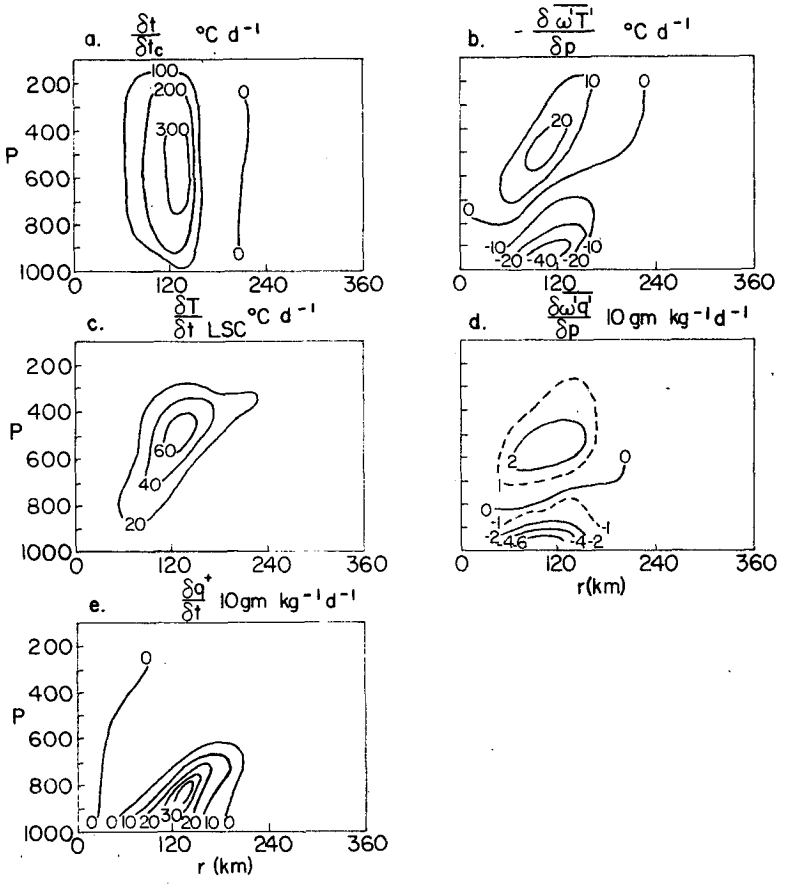

FIG. 12. Vertical cross sections at 72 h of (a) convective heating term $\partial T/\partial t_c$, (b) vertical eddy flux heating term $\partial \overline{\omega' T'}/\partial p$, (c) large-scale heating term $\partial T/\partial t_{LSC}$, (d) vertical eddy moisture flux term $-\partial \overline{\omega' q'}/\partial p$ and (e) convective moistening term $\partial q^+/\partial t$.

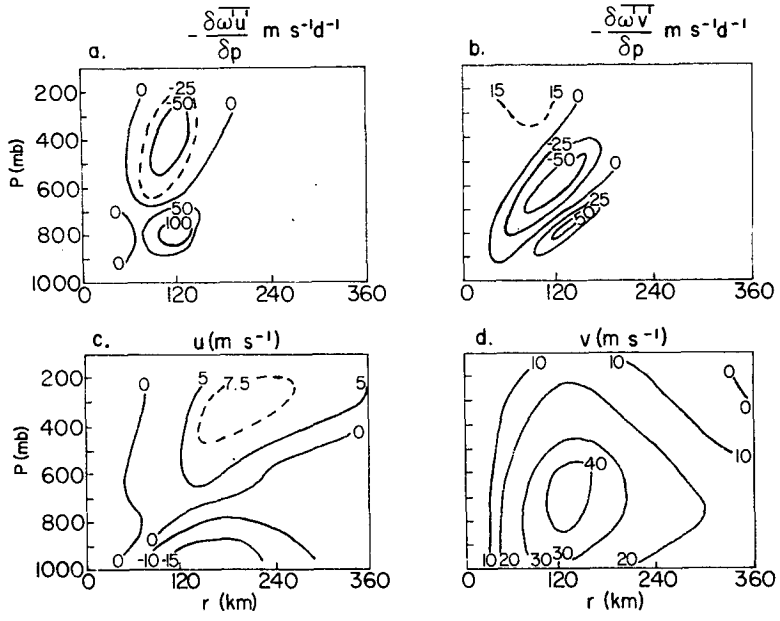

FIG. 13. Vertical cross sections at 72h of (a) divergence of vertical eddy flux of radial momentum $-\partial\overline{\omega'u'}/\partial p$ (b), divergence of vertical eddy flux of tangential momentum, $-\partial\overline{\omega'v'}/\partial p$, (c) radial wind component u and (d) tangential wind component v.

An explicit representation of the vertical eddy fluxes of heat, moisture and momentum is included in the parameterization scheme, which permits quantitative study of the effect of these processes on mesoscale systems. In the hurricane model experiment, the fluxes of heat and moisture cooled and dried the lower troposphere while they warmed and moistened the upper troposphere. An important consequence of this vertical redistribution of energy was the shifting of the total heating maximum to a higher level, a requirement for development of a realistic hurricane structure. The low-level drying also acted to increase the storm's intensity by increasing the total evaporation rate.

The vertical transport of radial momentum by cumulus convection was relatively unimportant compared to the other terms in the radial equation of motion. However, the transport of tangential momentum was of the same order as the other terms in the tangential equation of motion. The major effect of the momentum transport by cumulus clouds, therefore, was to reduce the vertical shear of the tangential wind.

Acknowledgments. I would like to acknowledge the stimulating discussions on hurricane modeling with Drs. Stanley Rosenthal, John Hovermale and James Hoke that contributed to this research. Jan Villistrigo capably typed the manuscript. This work was supported by NOAA Grant 04-4-022-26 and NOAA Contract 03-6-021-35106.

REFERENCES

Anthes, R. A., 1972: The development of asymmetries in a three-dimensional numerical model of the tropical cyclone. *Mon. Wea. Rev.*, **100**, 461–476.

——, 1977: A cumulus parameterization scheme utilizing a one-dimensional cloud model. *Mon. Wea. Rev.*, **105**, 270–286.

——, S. L. Rosenthal and J. W. Trout, 1971a: Preliminary results from an asymmetric model of the tropical cyclone. *Mon. Wea. Rev.*, **99**, 744–758.

——, J. W. Trout and S. L. Rosenthal, 1971b: Comparison of tropical cyclone simulations with and without the assumption of circular symmetry. *Mon. Wea. Rev.*, **99**, 759–766.

Bergman, K. H., and T. N. Carlson, 1975: Objective analysis of aircraft data in tropical cyclones. *Mon. Wea. Rev.*, **103**, 431–444.

Gray, W. M., 1967: The mutual variation of wind, shear and baroclinicity in the cumulus convective atmosphere of the hurricane. *Mon. Wea. Rev.*, **95**, 55–73.

Hebert, P. J., and C. L. Jordan, 1959: Mean soundings for the Gulf of Mexico area. NHR4 Rep. No. 30, 10 pp. [Available from National Hurricane and Experimental Laboratory, Coral Gables, Fla.]

Hovermale, J., D. Marks, R. Chu, S. Scolnik and R. Jones, 1975: Experimental forecasts of hurricane movement with a limited area fine mesh grid. Paper presented at Ninth Tech. Conf. Hurricanes and Tropical Meteorology, 27–30 May, Miami, Fla. (Abstract in *Bull. Amer. Meteor. Soc.*, **56**, 326.)

Koss, W. J., 1976: Linear stability of CISK-induced disturbances: Fourier component eigenvalue analysis. *J. Atmos. Sci.*, **33**, 1195–1222.

Kurihara, Y., and R. E. Tuleya, 1974: Structure of a tropical cyclone developed in a three-dimensional numerical simulation model. *J. Atmos. Sci.*, **31**, 893–919.

Kuo, H. L., 1965: On formation and intensification of tropical cyclones through latent heat release by cumulus convection. *J. Atmos. Sci.*, **22**, 40–63.

——, 1974: Further studies of the parameterization of the influence of cumulus convection on large-scale flow. *J. Atmos. Sci.*, **31**, 1232–1240.

Malkus, J. S., C. Ronne and M. Chaffee, 1961: Cloud patterns in Hurricane Daisy. *Tellus*, **13**, 8–30.

Mathur, M. B., 1974: A multiple-grid primitive equation model to simulate the development of an asymmetric hurricane (Isbell, 1964). *J. Atmos. Sci.*, **31**, 371–393.

Matsuno, T., 1966: Numerical integrations of the primitive equations by a simulated backward difference method. *J. Meteor. Soc. Japan*, **44**, 76–84.

Miller, B. I., P. Chase and B. Jarvinen, 1972: Numerical prediction of tropical weather systems. *Mon. Wea. Rev.*, **100**, 825–835.

Rosenthal, S. L., 1970: Experiments with a numerical model for tropical cyclone development. Some effects of radial resolution. *Mon. Wea. Rev.*, **98**, 106–120.

——, 1971: The response of a tropical cyclone model to variations in boundary layer parameters, initial conditions, lateral boundary conditions and domain size. *Mon. Wea. Rev.*, **99**, 767–777.

Smagorinsky, J., S. Manabe and J. Holloway, Jr., 1965: Numerical results from a nine-level general circulation model of the atmosphere. *Mon. Wea. Rev.*, **93**, 727–768.

Yamasaki, M., 1968: Numerical simulation of tropical cyclone development with the use of primitive equations. *J. Meteor. Soc. Japan*, **46**, 178–210.